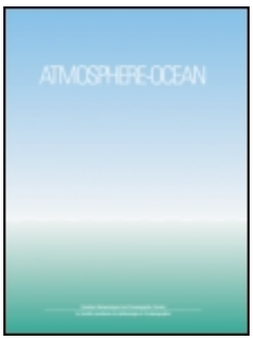

Atmosphere-Ocean

ISSN: 0705-5900 (Print) 1480-9214 (Online) Journal homepage: https://www.tandfonline.com/loi/tato20

# A simple gravity wave drag parametrization for use in medium-range weather forecast models

C. Chouinard , M. Béland & N. McFarlane

**To cite this article:** C. Chouinard , M. Béland & N. McFarlane (1986) A simple gravity wave drag parametrization for use in medium-range weather forecast models, Atmosphere-Ocean, 24:2, 91-110, DOI: 10.1080/07055900.1986.9649242

**To link to this article:** https://doi.org/10.1080/07055900.1986.9649242

# A Simple Gravity Wave Drag Parametrization for Use in Medium-Range Weather Forecast Models

C. Chouinard and M. Béland
*Recherche en prévision numérique*
*Atmospheric Environment Service*
*Dorval (Quebec) H9P 1J3*
and
N. McFarlane
*Canadian Climate Centre*
*Atmospheric Environment Service*
*Downsview, Ontario M3H 5T4*

[Original manuscript received 7 October 1985; in revised form 7 April 1986]

ABSTRACT *A simple gravity wave drag parametrization over mountainous terrain is tested for its ability to reduce the systematic errors of medium-range weather forecasts. Following Boer et al. (1984), this parametrization is a function of the low-level wind speed and stability, the local Froude number, and the variance of the subgrid-scale orographic features.*

*A comparison study of ten 7-day forecasts obtained with envelope orography, wave drag or standard orography, shows that wave drag is as effective as envelope orography in reducing the systematic errors. A further comparison where the combined effects of the wave drag and that of a complementary enhanced orography (that is one that includes only the subgrid-scale elements not treated separately by wave drag) are taken into account shows this latter approach to be the most promising in reducing orographically-related systematic errors.*

RÉSUMÉ *On étudie le pouvoir d'une paramétrisation simple de la résistance des ondes de gravité, dans une région montagneuse, à réduire les erreurs systématiques des prévisions météorologiques à moyenne échéance. On adopte l'approche de Boer et al. (1984) qui exprime cette paramétrisation en fonction du vent et de la stabilité à basse altitude, du nombre de Froude local, et de la variance des caractéristiques orographiques aux échelles inférieures à celle de la grille.*

*Une étude comparant 10 prévisions de 7 jours chacune, obtenues à partir d'une enveloppe orographique, et à partir de résistance d'onde ou orographie standard, montre que la résistance d'onde est aussi efficace que l'enveloppe orographique à réduire les erreurs systématiques. Une autre comparaison où sont pris en considération les effets combinés de la résistance de l'onde, et d'une orographie complémentaire développée (c.-à.-d. qui inclue seulement les éléments aux échelles inférieures de celle de la grille et qui ne sont pas traités séparément par la résistance d'onde) indique que cette dernière approche est meilleur candidat pour la réduction des erreurs systématiques associées à l'orographie.*

*ATMOSPHERE-OCEAN 24* (2) 1986 91–110 0705-5900/86/0000-0091$01.25/0

## 1 Introduction

Mid-latitude systematic errors in numerical models are probably one of the major problems that will have to be solved if the accuracy of medium-range numerical forecasts is to be increased in any significant fashion. A lot of attention has been paid to this subject recently: A good review can be found in Sadourny (1984); specific examples related to particular large-scale models are given in Wallace et al. (1983) (hereafter denoted WTS), for the European Centre model, and in Chouinard (1984) for the Recherche en prévision numérique (RPN) model.

In this paper, we focus our attention on two particular (possibly related) types of systematic errors, the general weakening of stationary planetary waves in the Northern Hemisphere winter, and the generation of strong westerlies across the Rocky Mountains and northwest Europe (along with a systematic northward displacement of the jet axis). We have yet to find a plausible cause or source for this type of error, and more than likely there is more than one source of error involved. What is evident from the studies already published on the topic is that there exists a close relationship between the location and amplitude of the error and the geographical distribution of fixed sources of heat and momentum, i.e. mountains and oceans. In this study we use a rather simple adiabatic model and consequently deal only with the errors that pertain to mechanical or mountain forcing. WTS, as noted earlier, have reported on this type of error in the European Centre model. They proposed and tested a rather novel concept for reducing this source of systematic error in their medium-range weather forecasts. It is based on the introduction of an enhanced orography that is now referred to as "envelope" orography. Their approach, although simple, even trivial in a sigma coordinate system, proved to be quite efficient. However, raising the bottom topography by as much as 2 km in some areas is not without problems in a numerical model with full physics. The delicate balance of the radiative processes in the planetary boundary layer can be significantly altered, not to mention that some major basins and valleys are completely filled in on going to the "envelope" orography. In a data assimilation cycle these could have undesirable effects leading to an unreasonably large amount of data being rejected. Thus the envelope solves some problems but not without causing some difficulties to some other aspects of the model.

Vertically propagating gravity waves excited at the surface when stable air flows over irregular terrain can exert an implicit drag on the large-scale flow and thereby effectively control the amplitude and position of forced planetary waves. Lilly (1972) was one of the first to hypothesize that gravity wave drag (GWD), because of its magnitude in regions of large mid-latitude massifs such as the Rockies, could effectively control the position and intensity of westerlies as simulated by general circulation models (GCM). He proceeded to show how sensitive a GCM was to the application of a crude parametrization of GWD. He concluded that the introduction of mountain-induced GWD could well have major impacts on both the short and long time-scales of any numerical model integration.

Recently, Boer et al. (1984) (hereinafter denoted as BMLB) have demonstrated how the use of yet another simple but efficient parametrization of orographically generated gravity wave drag effects can result in improved GCM simulations. The

improvements noted by these authors were similar in nature to those that have been found by WTS in association with the use of envelope orography. Thus it is possible that use of a simple gravity wave drag parametrization may lead to improved medium-range weather forecasts as well.

Given the success noted by BMLB from the introduction of gravity wave drag effects in their GCM in alleviating some of the major problems of their simulations, and given its similarity to the systematic errors of medium-range forecasts, we decided to test a variant of their GWD parametrization in a global version of the RPN spectral model in an attempt to reduce its systematic errors.

In the next section we will present the GWD parametrization scheme. In Section 3 we will briefly describe how we derived the envelope orography and a new field called the "launching height," which is required in the GWD approach. In Section 4 we will discuss the most interesting results of this study, and in Section 5 we will draw some conclusions from this work.

## 2 Parametrization of Wave Drag effects

Vertically propagating gravity waves can be excited when stable air flows over irregular terrain. These waves transport momentum between their source regions near the surface and regions where they are dissipated or absorbed. The momentum flux divergence that occurs in regions of dissipation or absorption acts to decelerate the large-scale flow.

As in BMLB we will assume that the momentum flux divergence associated with the gravity waves acts opposite to the large-scale flow at some reference level near the surface. Denoting large-scale flow quantities at that level by a zero subscript, the momentum flux at the surface is represented as follows:

$$\tau = -\alpha h_e \rho_0 N_0 \mathbf{V}_0,$$

where $\rho$, $N$, $\mathbf{V}$ are air density, Brunt-Väisälä frequency, and horizontal velocity, respectively. The quantity $h_e$ is an effective subgrid-scale orographic perturbation amplitude while the dimensionless parameter $\alpha$ is taken to be a constant whose value is to be determined empirically.

Momentum flux divergence occurs in regions where waves are subject to dissipation associated with the development of smaller scale turbulent motions. These turbulent motions may occur in association with the development of unstable shear zones or static instabilities. Such instabilities may be expected in regions where the waves have sufficient amplitudes that the slopes of the streamline displacements associated with them are close to unity in magnitude. As discussed in BMLB this is approximately true when the Froude number is of order unity. This quantity is defined as follows:

$$\mathrm{F} = \frac{N h_e}{U} \left\{ \frac{\rho_0 N_0 U_0}{\rho N U} \right\}^{1/2}$$

where the velocity $U$ is associated with that component of the local flow that is parallel to the reference level flow, i.e.

$$U = \frac{\mathbf{V} \cdot \mathbf{V}_0}{|\mathbf{V}_0|}.$$

The vertical structure of F is typically such that it decreases slightly with height (due to increases in wind speed throughout the troposphere) and then increases rapidly with height in the lower stratosphere. Over high, rough terrain the Froude number tends to increase rapidly from above the tropopause. Thus it is to be expected that wave drag effects may be important in the upper troposphere and lower stratosphere.

The Froude number may quite often be of order unity near the surface as well. In such circumstances a number of effects may be important. Non-linear effects due to finite orographic perturbations may lead to enhancement of surface stresses above values estimated on the basis of linear theory (while at the same time suppressing the tendency for convective overturning near the surface). On the other hand the incoming flow near the surface upstream from orographic peaks may be partially decelerated and diverted around obstacles. This upstream blocking effect would tend to reduce the effective obstacle height for flow over the mountains. However, the flow downstream from obstacles may be strongly accelerated owing to the descent of stable air on the leeward slopes.

The recent work by Pierrehumbert and Wyman (1985) suggests that in such circumstances the occurrence of upstream flow deceleration may be intimately connected with the onset of gravity wave breaking due to convective overturning. For two-dimensional flows the magnitude of the upstream deceleration near the surface depends both on the Froude number and the Rossby number defined as

$$\mathrm{Ro} \equiv U/fL$$

where $U$ is the incoming flow speed near the surface upstream from the blocked region and $L$ is a typical obstacle half width.

When Ro is less than unity the upstream deceleration is dependent on the product RoF and hence is independent of the speed of the incoming flow. However when Ro is of the order of unity or larger the deceleration is proportional to F alone provided this parameter is large enough to ensure that wave breaking can occur within a distance of the order of a vertical wavelength above the upstream surface. Hence in this regime the upstream deceleration is inversely proportional to the speed of the incoming flow. Also the downstream flow is strongly accelerated in a narrow region near the surface. The recent studies of Peltier and Clark (1979, 1983) indicate that in these circumstances large momentum flux divergences may occur in the lower troposphere in association with amplification of the gravity wave between the surface and the level where convective instability first occurs.

The extent to which these results may be representative of more general conditions involving three-dimensional flows is not known. It is reasonable to conclude, however, that in a small Rossby number regime gravity wave radiation and wave drag effects would be of secondary importance to those due to the mountain barrier effect, which causes upstream deceleration and flow diversion. The theory suggests that in these circumstances the barrier effect is predominantly a function of mountain slope and hence is substantially reduced by use of smoothed orography. The use

of envelope orography as outlined by WTS represents a simple way of partially maintaining this barrier effect.

The large Rossby number regime is one where the effects of upstream blocking and gravity wave drag are probably intimately related to each other. Unfortunately, the available theory provides little guidance in the matter of representing the combined effects of these processes on the large-scale flow near the surface. In higher regions where F is increasing with height the "wave saturation" ideas recently discussed by Lindzen (1981) provide a useful basis for representing wave drag effects. One of the present authors (NAM) has recently developed a parametrization based on these ideas. This scheme is (at the time of writing) being tested in the AES general circulation model and will be reported on elsewhere.

In the present work a much simpler approach is used. It is assumed that there will be a retardation of the large-scale flow in regions where the Froude number exceeds some critical value of the order of unity. If, in the model, this criterion is not satisfied below the highest model level then all drag effects are assumed to occur there. A further constraint will be that all drag effects are confined to the region between the reference level and the lowest level where $U$, as defined above, vanishes. This will account for critical-layer absorption.

The effective drag force is assumed to act opposite to the flow at the reference level and gives rise to an acceleration term which is represented as follows:

$$\left(\frac{\delta \mathbf{V}}{\delta t}\right)_{\text{GWD}} = -\lambda U^2 \frac{\mathbf{V}_0}{|\mathbf{V}_0|} \max\left\{1 - \delta \frac{\mathrm{F}_c^2}{\mathrm{F}^2}, 0\right\}, \quad \sigma_0 \leqslant \sigma \leqslant \sigma_c$$

$$= 0; \quad \text{elsewhere}$$

where $U$ is as defined above and is positive in the region between the reference level and $\sigma_c$, but negative or zero above that point. The quantity $\delta$ is zero at the top level of the model and unity elsewhere.

The parameter $\lambda$ is determined by requiring that

$$\int_{\sigma_0}^{\sigma_c} \rho \left(\frac{\delta \mathbf{V}}{\delta t}\right)_{\text{GWD}} d\sigma = \boldsymbol{\tau}_0$$

giving

$$\lambda = \frac{\alpha h_e \rho_0 N_0 |\mathbf{V}_0|}{\int_{\sigma_0}^{\sigma_c} U^2 \max\left(1 - \delta \frac{\mathrm{F}_c^2}{\mathrm{F}^2}, 0\right) d\sigma}$$

In the experiments that have been carried out the parameter settings were $\mathrm{F}_c^2 = 0.5$ and $\alpha = 0.01$. The amplitude $h_e$ was set equal to twice the standard deviation associated with subgrid-scale orographic variations for a latitude-longitude grid resolution of 1.875 degrees. This resolution limit was chosen to correspond roughly to that which is dictated by the assumption that Coriolis effects are negligible in the gravity wave dynamics. This implies that horizontal wavelengths will usually be no longer than about 600 km in middle latitudes. Wave drag effects are negligible for wavelengths that are much longer than this limit.

Although the above wave drag parametrization is not based on a specific hypothesis (such as wave saturation) concerning the effects of dissipation on the waves, it does account, in a crude but simple way, for some of the main effects of such processes. In particular, in regions where $F/F_c$ is greater than unity and increasing with height, wave drag effects are confined to the region bounded by the lowest critical level (or the top of the model if $U > 0$ everywhere) and the point at which $F/F_c$ is unity. If (as may often be the case) $F/F_c$ exceeds unity near the surface but decreases to less than unity in the middle or upper part of the troposphere, some drag effects will be felt in the lower troposphere. This accounts crudely for the possibility that there may be enhanced momentum flux divergence in association with partial blocking and/or temporal amplification of the wave in the lower troposphere. In some earlier experiments these effects were arbitrarily eliminated by restricting the magnitude of $h_e$ so as to ensure that the ratio $F/F_c$ would not exceed unity at the reference level. The results of those experiments led to the conclusion that it is useful to allow some drag effects to occur in the lower troposphere.

The chosen value of $\alpha$ was obtained by numerical experimentation. Over mountainous regions, such as the Rockies, where $h_e$ is of the order of 1 km or more this choice gives values of $|\tau_0|$ in the range of 1–10 dynes $cm^{-2}$. Values of this magnitude, though somewhat larger than those typically observed (Lilly et al., 1982), are not uncommon. Values considerably larger than this have been observed (Lilly, 1978). Moreover in these circumstances $F/F_c$ is usually greater than unity near the surface so that, according to the chosen representation, substantial stress divergence will occur in the lower troposphere. This effect is likely to be most pronounced over high, rough terrain when lower tropospheric wind speeds are of substantial magnitude.

It is unlikely that this simple parametrization will adequately account for all of the important flow modification effects near the surface. This is certainly true in the low Rossby number regime where gravity wave drag effects are negligible. In the high Rossby number regime as well, it may be desirable to introduce, in addition to the wave drag parametrization, some way of accounting for the low-level barrier effect of subgrid-scale orography. However, the available theoretical knowledge does not suggest a simple way to do this. Hence in this study no attempt, beyond that described above, will be made to account for the combined effects of wave drag and low-level blocking.

In one of the sets of forecast experiments to be described further in Section 4, a combination of envelope orography and wave drag parametrization was used. In that set of experiments the envelope used for orographic enhancement was based on the orographic variance in those subgrid scales for which the effective Rossby number is likely to be less than unity. The *remainder* of the subgrid-scale variance was used to construct gravity wave launching heights in the manner described in subsection 3b below. An additional set of experiments using envelope orography alone (no wave drag) was also performed. For this set of experiments all of the subgrid-scale orographic variance was used to construct the envelope orography.

## 3 Production of the envelope orography and the launching height fields

### a *Production of the Envelope Orography*

Most of the studies dealing with systematic errors point to a possibly rather serious underestimate of the planetary wave forcing by the mountains and/or land-sea contrast. This is particularly evident from the space-time behaviour of the long-wave error of medium-range weather forecasts (Chouinard, 1984). There is a clear indication of a systematic loss of amplitude and/or geographical adjustment in each and every forecast. Since the amplitude of the forced planetary waves is directly related to the amplitude and horizontal scale of the underlying topography, it would appear that one could partially resolve the problem by simply enhancing the orographic features of the model. This is exactly what was proposed by Mesinger (1977) and Bleck (1977) in the context of Genoa cyclogenesis and was subsequently used by WTS to alleviate the systematic errors of the ECMWF model.

As in WTS, we have linearly related the incremental enhancement to the subgrid-scale standard deviation with a factor of 2.0. The high-resolution U.S. Navy data set was used for calculating the standard deviation. Specifically we have calculated the standard deviation of the subgrid scales with respect to the model grid-averaged $h$ as,

$$\sigma = \left\{ \frac{\sum_i p_i (h_i - \bar{h})^2}{\sum_i p_i} \right\}^{1/2},$$

and like WTS, we have added a further correction to the above to account for the unresolved feature of even the high-resolution data set as,

$$\sigma^* = \left\{ \frac{\sum_i p_i (h_i^{\max} - \bar{h}_i)(\bar{h}_i - h_i^{\min})}{\sum_i p_i} \right\}$$

where $h_i^{\max}$, $h_i^{\min}$ and $\bar{h}_i$ refer, respectively, to the maximum, minimum and average reported terrain heights within each of the $i$th grid squares of the high resolution U.S. Navy data set, and $p_i$ is its relative weight. The model grid averaged height $\bar{h}$ is defined as,

$$\bar{h} = \frac{\sum_i p_i h_i}{\sum_i p_i}$$

Since we are planning an experiment with a spectral model truncated at 42 waves, the model grid about which the standard deviation was calculated is a Gaussian latitude-longitude grid with 128 points and 64 points in the east-west and the north-south directions, respectively.

The envelope orography resulting from this first step was then spectrally smoothed by successively transforming it from spectral to grid space intermediately setting

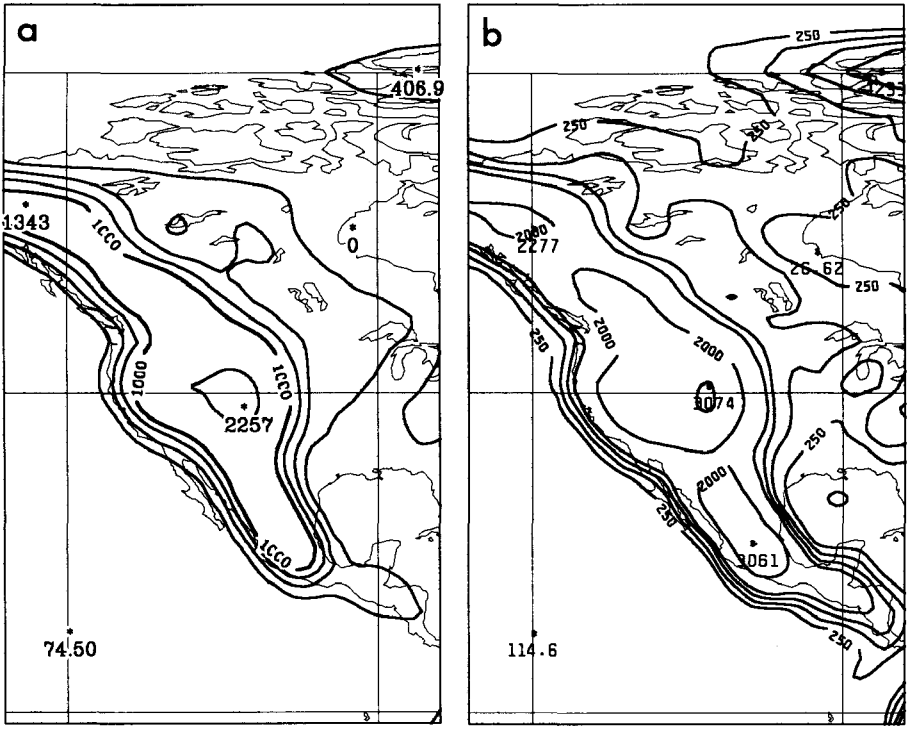


Fig. 1 (a) Standard and (b) envelope orographies for the Rockies. Both are triangularly truncated at wavenumber 42, and have been smoothed (see text, Section 3a). Contour interval: 250 m up to 1000 m and 1000 m above.

all negative values to zero on the Gaussian grid. A total of 15 such full transforms were carried out to smooth the field. This smoothing operation is not without side effects, such as raising the mean height and extending the continental boundary over the waters, but it is necessary to remove some odd short-scale features that appear because of our rather simplistic approach to enhancing the orography. WTS subjected their envelope orography to a Gaussian-type smoother. Both types of smoothing were tested in this study, and we concluded from looking at 7-day forecasts prepared with both, that either produced results of comparable overall quality.

In Figs 1 and 2 we present the standard and envelope orographies at 42 waves resolution over the Rockies and Himalayas. It is interesting to note how the mountain ranges of the envelope orography are broader and how the peaks have effectively been raised in the process. As an example, the Sierra Mountains in Mexico have doubled in amplitude. Over the Himalayas the enhancement is generally of the order of 1 km, a fairly small value considering the highest peaks of the world are found in that area. This was to be expected since there is very little subgrid-scale variance over the plateau. Generally the enhancement around plateaus, such as Tibet and Greenland follows the edges where the gradient is steepest.

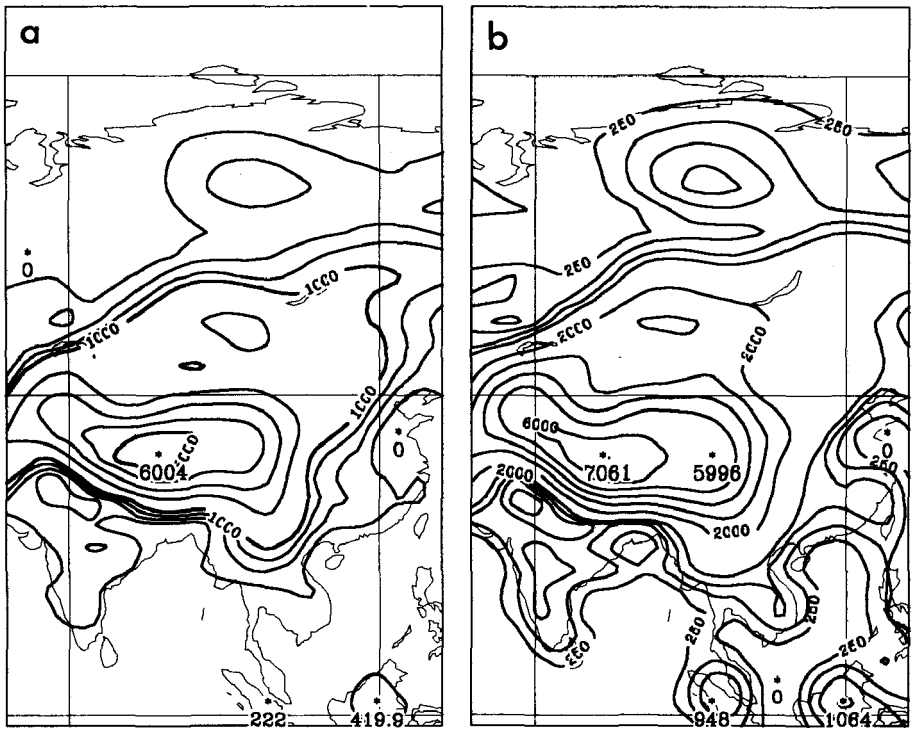


Fig. 2 Same as Fig. 1, except for the Himalayas.

In Fig. 3 we present profiles of the envelope and the standard orographies over North America and Eurasia. It is evident from the profiles that the higher the terrain the larger the increases. There are few exceptions, such as over the Caucasus where the increases are much larger than anticipated from looking at the standard orography. This is an area where we have noted large systematics errors and consequently this enhancement is highly desirable.

**b** *Production of the Launching Height*

In order to implement the wave drag parametrization, the "launching height" $h_e$ must be determined. As mentioned in the preceding section this parameter is also taken to be a measure of the subgrid-scale variance within a grid square of the model and as such is very closely related to the incremental enhancement we calculated to form the envelope orography, the most significant difference between the two being in the subgrid scales to be considered. Since the most effective scales in generating gravity waves are in the 10–100 km range, this meant evaluating the launching height about a global 192 × 96 Gaussian grid. In spectral space this meant all information beyond wavenumber 63 contained in the high resolution was effectively used for the launching height. As for the envelope orography, the incremental height, the launching height in this case, was linearly related to the standard deviation with a factor of 2.0.

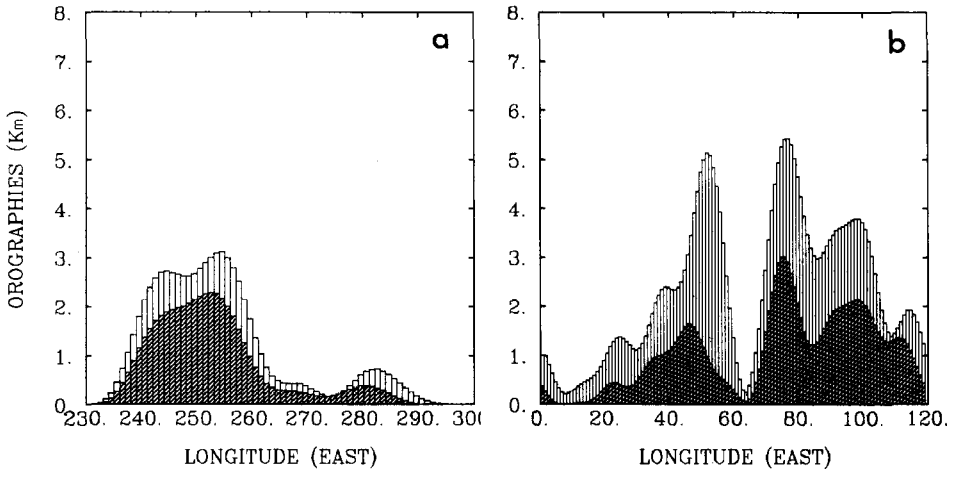


Fig. 3 East-west profiles of the standard (shaded) and envelope (clear) orographies: (a) Rockies, (b) Himalayas.

In Fig. 4 we present a window of the launching field over the Rockies. This field is as noisy as the unsmoothed envelope orography, and it is not clear whether it should be smoothed or not, nor is it clear what type of smoother should be applied to this field. This field comes in the problem rather indirectly, somewhat like a drag coefficient and some noise can be tolerated, more so than the orography itself. In an attempt to determine the net impact that smoothing the launching height would have on the forecasts, we prepared a series of 7-day forecasts with and without smoothing, holding everything else the same. The results from the test were quite conclusive and indicated a net deterioration in predictability when using the smoothed version of the field. We concluded that it is better to calculate the GWD as accurately as possible even though it is noisy and let the model handle the small-scale character of the forcing term. We realize that we are dealing with a rather robust spectral model and such an approach might not be adequate for other types of models.

### c *Model and Data*

The model used for this study is a global version of the RPN spectral model with triangular truncation at 42 waves. It uses linear finite elements in the vertical at 15 equally spaced levels starting at $\sigma = 1.0$ at the bottom and extending to $\sigma = 0.09$ at the top. The model was run adiabatically with a dry convective adjustment scheme and the simple Cressman drag formulation for surface friction. For a more complete description, the reader is referred to Béland and Beaudoin (1985).

The data used for this study were the FGGE-IIIb analyses set for the winter period 1978–1979 (December-January-February). We selected a total of ten cases, which we feel is a minimum set from which to draw any firm conclusions. Three of the cases were recommended by the FGGE Working Group on Numerical Experimentation and the seven others were chosen so as to separate each case from the other by a period of about ten days. Thus, each case is somewhat independent of the others. The list of the ten cases is given in Table 1.

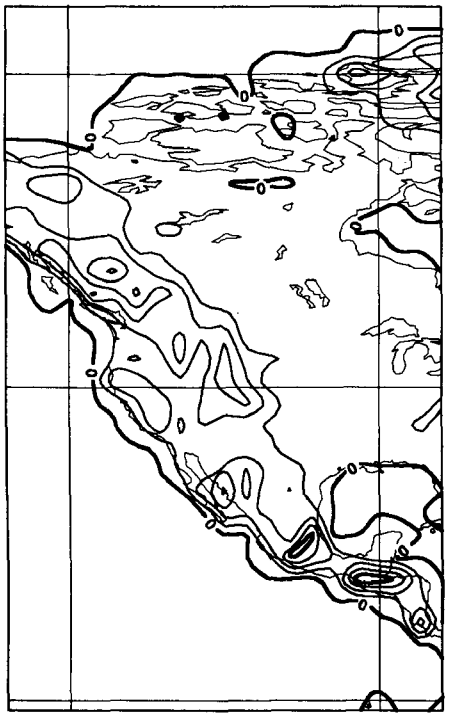

Fig. 4 Launching height field (see text, Section 3b for definition) over the Rockies. Contour interval: 250 m.

## 4 Results

We will now present the results of four groups of ten 7-day forecasts, made from the cases listed in Table 1. The first group of forecasts was made with what we shall call the standard orography (hereafter abbreviated STAN): It is simply the mountain field spectrally analysed at the model triangular truncation of 42. The second group used the envelope orography (hereafter abbreviated ENV) constructed in the manner described in Section 3. The third group used the standard orography with the gravity wave drag parametrization (hereafter abbreviated GWD) given in Section 2. Finally the fourth group used a combination of envelope orography and gravity wave drag (hereafter abbreviated GWD + ENV).

### a *Root-Mean-Square Height Errors (RMSE)*

We have plotted in Fig. 5 the average over the ten cases and over seven pressure levels extending from 1000 to 200 mb of the root-mean-square geopotential height error (RMSE in metres) for the Northern Hemisphere as a function of the forecast lengths in days. (The corresponding FGGE-IIIb analyses were used to compute these errors.) There are four different curves in the graph: From the coarse dashed line to the full line, by decreasing order of dash lengths, we have GWD, GWD + ENV, STAN and ENV. We observe that from day 0 to approximately day 3, GWD scores best, whereas ENV and GWD + ENV have the worst performance. This result for ENV was also noted in WTS. From day 3 to 7, the situation reverses, and the best results are now obtained with ENV and GWD + ENV, followed

TABLE 1. Initial time for the 10 integrations

| Year | Month | Day | Time (GMT) |
|---|---|---|---|
| 1978 | December | 14 | 00 |
| | | 21 | 00 |
| | | 26 | 12 |
| 1979 | January | 2 | 00 |
| | | 15 | 12 |
| | | 21 | 12 |
| 1979 | February | 5 | 12 |
| | | 12 | 12 |
| | | 17 | 00 |
| | | 24 | 00 |

closely by GWD. The gain in predictability over STAN (as determined by the time at which the RMSE equals 100 m) is half a day, again a value quite typical of WTS. We note the very similar performance of GWD and ENV, in terms of RMSE, when compared to STAN. This does not necessarily imply that the impact of GWD and ENV is similar from forecast to forecast. An example is shown in Figs 6a–d, where we have plotted the 500-mb (a, b) and 1000-mb (c, d) geopotential height forecasts at day 5 for the case integrated from the 12 February 1979, 12 GMT analysis; the top graph is for GWD, and the bottom for ENV. The flow structure at 500 mb off the Gulf of Alaska is quite different in the two simulations, and we note the presence of a well defined low at the surface in ENV that is missing in GWD. Similar differences appear on the eastern side of the block centred over Norway. For this particular synoptic situation, the verification (not shown) favors the ENV simulation, although it is fair to say that both ENV and GWD are much more similar to each other than to the verifying analysis.

**b** *Systematic 500-mb Height Errors*

Figures 7a–d show the systematic 500-mb height error in metres for STAN, ENV, GWD and GWD + ENV in that order, at day 7. It is obtained by subtracting the mean of the 10 verifying analyses from the mean of the ten corresponding 7-day forecasts. Thus a positive (negative) value indicates an overestimate (underestimate) of the corresponding forecast ridge or trough. The pattern displayed in Fig. 7a is quite typical (see WTS, or Chouinard, 1984): We observe, for example, an underestimate of the ridge amplitude over the Rockies; too much zonality over western Europe; where the error of $-179$ m is reduced to $-120$ m for ENV and $-94$ m for GWD; on the east coast, with 128, 83 and 101 m; and over the Rockies, with $-163$, $-141$ and $-151$ m. For this particular error pattern, both GWD and ENV seem to produce rather similar improvements.

We note, however, an important increase over northern Siberia for both ENV and GWD, whereas other centres appear totally insensitive to either ENV or GWD

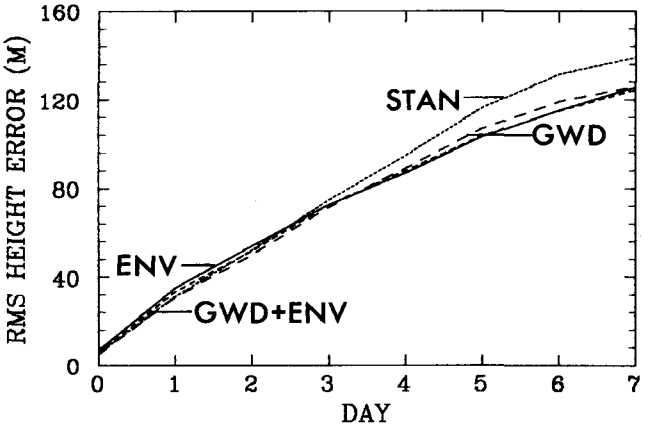


Fig. 5 Root-mean-square geopotential height error (m) averaged over ten cases and seven pressure levels (from 200 to 1000 mb), for the Northern Hemisphere, as a function of forecast length in days. From coarse dashed line to full line, by decreasing dash-length, we have gravity wave drag (GWD), gravity wave drag and envelope (GWD + ENV), standard (STAN) and finally envelope (ENV).

(for example, the 132-m error over the Aral Sea). This would seem to confirm that systematic errors are probably caused by a combination of different model defects and/or inaccuracies, the balance of which is tilted in the right direction over certain areas, and in the wrong direction in other areas, when one tries to correct one aspect at a time of these defects and/or inaccuracies. This is further exemplified in Fig. 7d, where we show the systematic error pattern of GWD + ENV. This particular combination seems to yield the best overall result, with a further reduction to $-131$ m over the Rockies, and $-69$ m over Europe.

**c** *Meridional Transport of Zonal Momentum*

We shall now focus our attention on the other important systematic error of the model, the generation of strong westerlies, and particularly the erroneous systematic northward displacement of the jet axis. One of the controlling factors in the correct positioning of the jet axis is the correct location (on average) of the convergence (or divergence) of the meridional transport of zonal momentum. We have plotted on Figs 8a–e the equator-to-pole cross-sections of the zonal average of this quantity at day 7, again for STAN, ENV, GWD, GWD + ENV and observed, in that order (units: $m^2 s^{-2}$). This quantity is denoted $\bar{u}'\bar{v}'$, where a prime denotes an instantaneous deviation from a zonal average, and the bar a zonal average; it has been evaluated at day 7 of each of the ten forecasts, followed by a simple average over the ten forecasts; the same was done for the ten verifying FGGE-IIIb analyses to produce Fig. 8e. A comparison of Fig. 8a and Fig. 8e shows that the model with a standard orography severely underestimates the transport: the northward positive transport has a maximum value of 15 instead of 25, and the southward negative transport is insignificant. Moreover, the positioning error results in a fictitious northward dis-

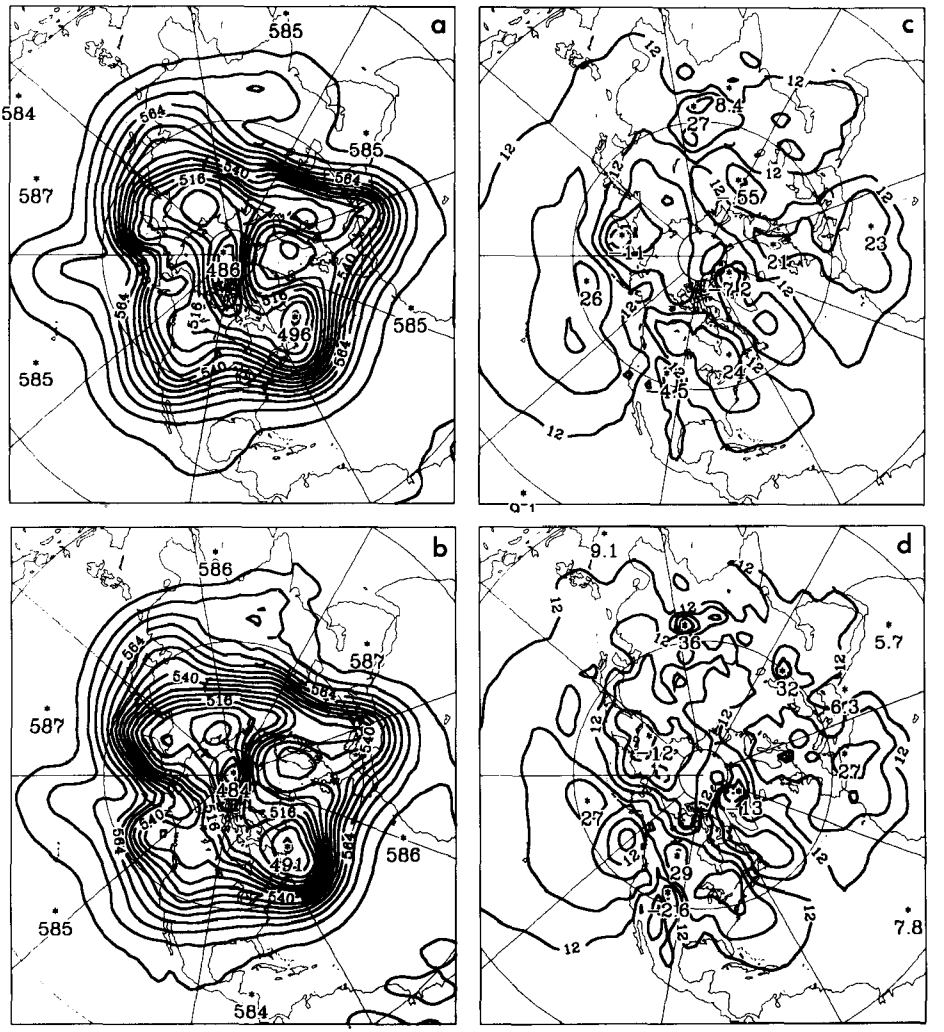


Fig. 6 The 500-mb height forecast on day 5 starting from 12 February 1979, 1200 GMT and using (a) the standard orography with gravity wave drag (GWD) and (b) using only the envelope (ENV) orography. Contour interval: 6 dam. (c) and (d): same as (a) and (b), except for the 1000-mb level.

placement of the maximum convergence zone, which in turn contributes to a fictitious northward displacement of the jet axis (this will be shown in the next subsection). Adding either ENV (Fig. 8b) or GWD (Fig. 8c) results in an increase of the southerly transport: We note, however, that although the increase is smaller for GWD, it seems to be better positioned when verified against Fig. 8e. The best overall result is again obtained with GWD + ENV, as can be seen in Fig. 8d: Although the maximum and minimum values are still underestimated by roughly 50%, the position of the convergence zone, as well as its strength, is much closer

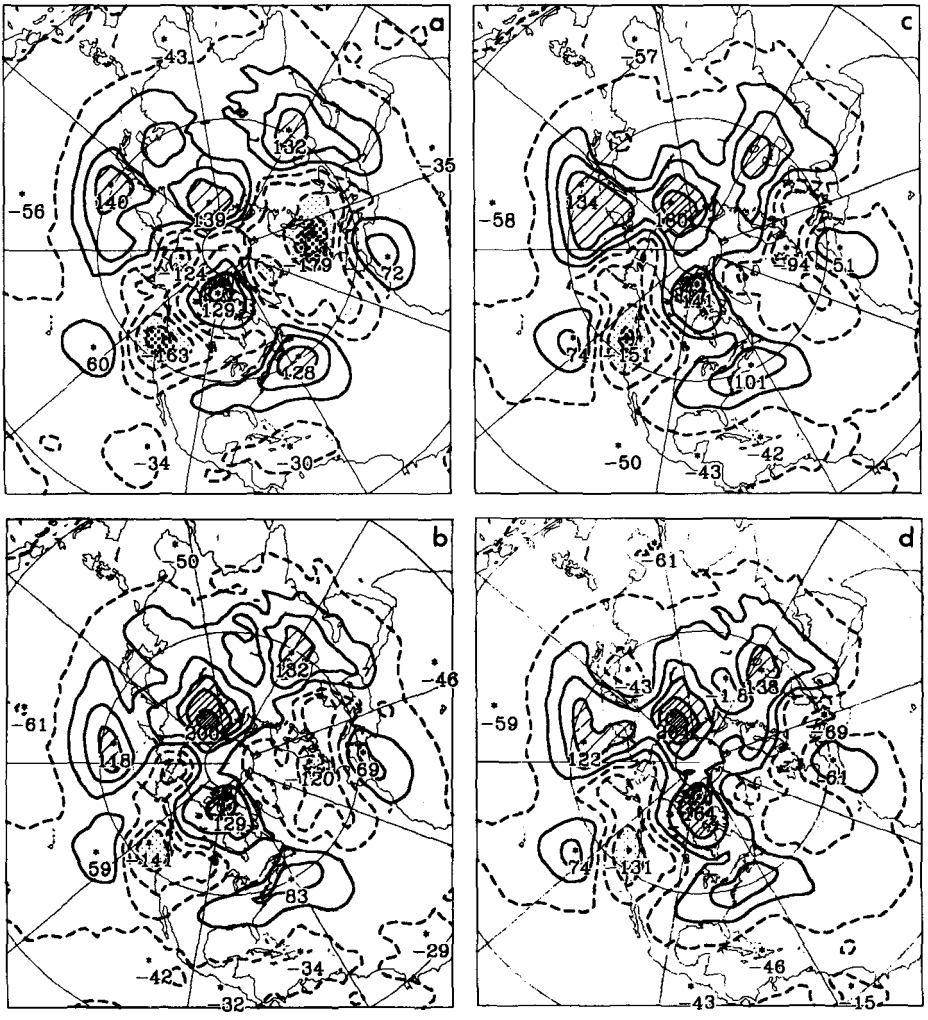


Fig. 7 Mean 500-mb height error in metres of day 7 forecasts, obtained by averaging the forecast minus the verifying analysis over the ten cases for (a) standard orography (STAN); (b) envelope orography (ENV); (c) gravity wave drag (GWD) and standard orography, and (d) gravity wave drag and envelope orography (GWD + ENV). Contour intervals are 40 m starting at ±20 m, with negative contours dashed.

to that depicted in Fig. 8e. This would imply a correct positioning, on the average, of the zonal wind acceleration, leading to a decreased fictitious northward jet axis displacement. An example of this follows.

**d** *Zonal Flow Cross-Section*

We have plotted in Figs 9a–e, the equator-to-pole cross-section of the zonal wind, taken at 0° longitude, at day 7, and averaged over the ten forecasts (units: m $s^{-1}$); the order is the same as for Fig. 8. Comparing Fig. 9a with Fig. 9e, we notice

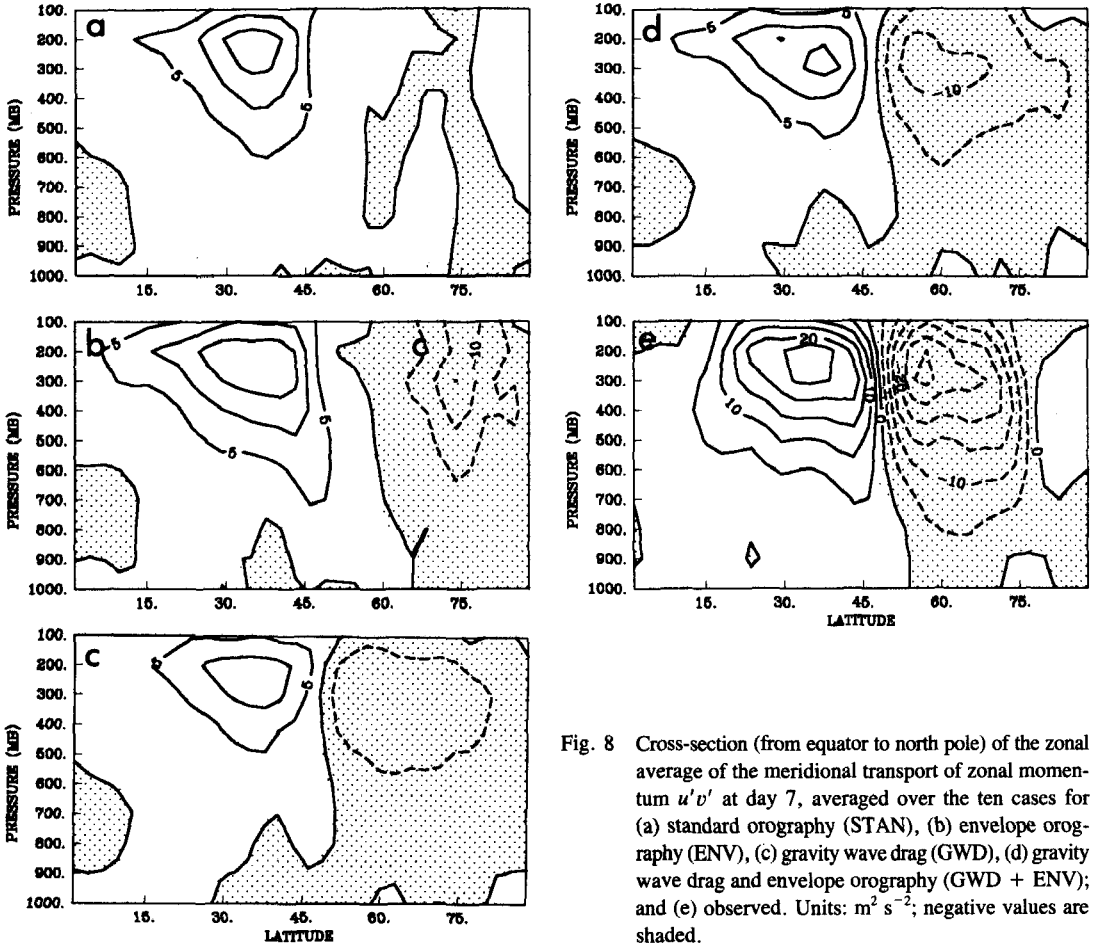


Fig. 8 Cross-section (from equator to north pole) of the zonal average of the meridional transport of zonal momentum $u'v'$ at day 7, averaged over the ten cases for (a) standard orography (STAN), (b) envelope orography (ENV), (c) gravity wave drag (GWD), (d) gravity wave drag and envelope orography (GWD + ENV); and (e) observed. Units: $m^2\ s^{-2}$; negative values are shaded.

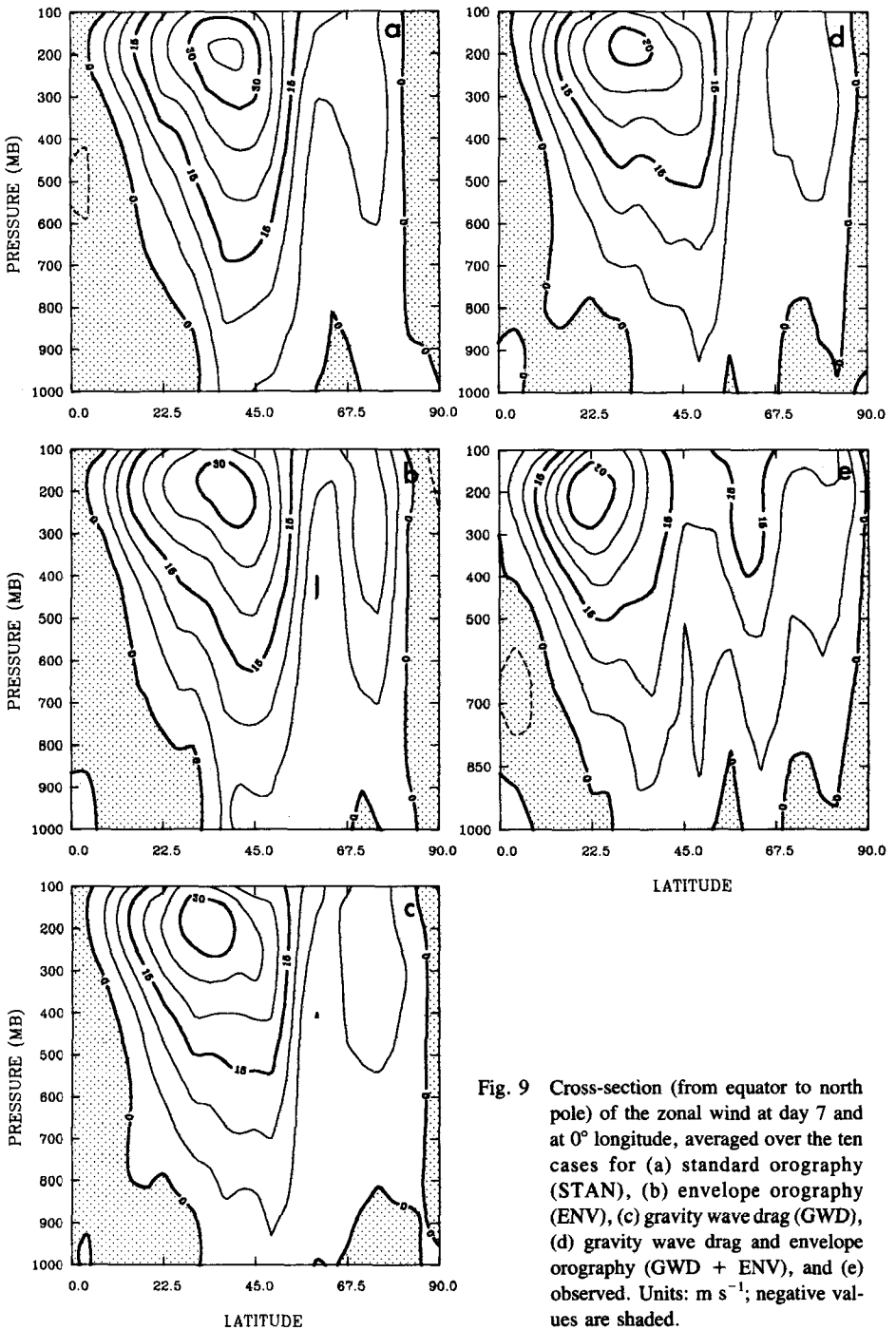


Fig. 9 Cross-section (from equator to north pole) of the zonal wind at day 7 and at 0° longitude, averaged over the ten cases for (a) standard orography (STAN), (b) envelope orography (ENV), (c) gravity wave drag (GWD), (d) gravity wave drag and envelope orography (GWD + ENV), and (e) observed. Units: m $s^{-1}$; negative values are shaded.

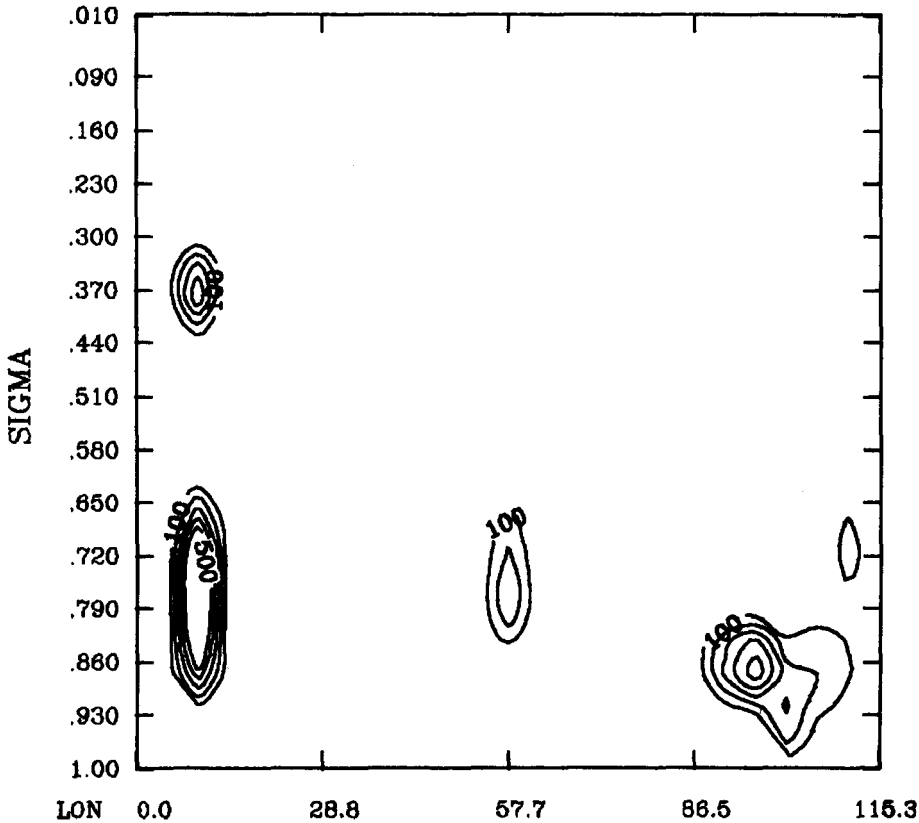


Fig. 10 Vertical cross-section taken at 27°N extending from 0 to 115.2°E of the instantaneous deceleration of the wind modulus caused by gravity wave drag, taken at day 1 of the 12 February 1979, 1200 GMT case. Contour interval: $100 \times 10^{-6}$ m s$^{-2}$.

immediately the large positional error of the jet axis, which is much too far to the north, and also the slight overestimation of the maximum wind speed (35 m s$^{-1}$ vs 30 m s$^{-1}$). As we go from Fig. 9b to Fig. 9c and Fig. 9d, e.g. from ENV to GWD to GWD + ENV, we notice a steady southward migration of the jet axis, thus reducing the error; there is also a 5 m s$^{-1}$ reduction of the maximum wind speed, which seems to agree quite well with the observed value of 30 m s$^{-1}$ in Fig. 8e. Again, the best overall result is obtained with the GWD + ENV combination, as can be easily verified by directly overlaying Figs 9b, c, d and e, in that order. This seems to confirm the preceding results discussed in subsection 4c.

**e** *Flow Deceleration*

Finally in order to give some idea of the magnitude and vertical distribution of the gravity wave drag during an integration, we show in Fig. 10 a vertical cross-section taken at latitude 27°N and extending from longitude 0° to 115.2°E of the wind modulus deceleration at day 1 of the 12 February 1979, 12 GMT case. To fix ideas,

a value of $-300$ m s$^{-2}$ corresponds roughly to a deceleration in wind speed of 1 m s$^{-1}$ h$^{-1}$. We do indeed observe instantaneous values of this order between the Ahaggar and Tibesti massifs in Africa, and over the Hindu Kush and the Himalayas. Note also the secondary maximum above the Ahaggar massif. Thus it seems that the gravity wave drag term is contributing where it should (e.g. near the mountain ranges), and produces instantaneous decelerations that are physically reasonable.

## 5 Conclusions

A simple gravity wave drag parametrization over mountainous terrain has been tested for its ability to reduce the systematic errors of medium-range weather numerical forecasts. Particular attention was given to the general weakening of stationary planetary waves in the Northern Hemisphere winter, and the generation of too strong westerlies across the Rockies and northwest Europe, along with a systematic northward displacement of the jet axis.

The first conclusion is that the GWD scheme alone is at least as good as an envelope orography in reducing the planetary wave systematic errors; moreover, it does not seem to deteriorate the early part of the forecast as the envelope does, and it does not introduce any complications near the surface, either in the boundary-layer package or the data assimilation package, due to "artificially" raised surface heights.

The second conclusion is that the GWD scheme alone seems to yield a better simulation of the Northern Hemisphere winter westerlies, particularly with respect to the positioning of the jet axis, than either the envelope or the standard orography. The reduction in the wind speed maximum appears, however, to be similar for both parametrizations.

The final and third conclusion is that the best overall results for the medium-range weather forecast model tested here are obtained by using a combination of both the GWD and the envelope orography. The particular combination tested here is as follows: Below a model truncation at wave number 60, one uses both an envelope orography (defined by adding to the model truncated orography the variance contained between wavenumber 60 and the model truncation wavenumber) and a launching height field for the GWD (using the variance between wavenumber 60 and the high-resolution mountain field input data set); 2° at and over a model truncation at wavenumber 60, one uses only the GWD.

## References


BÉLAND, M. and C. BEAUDOIN. 1985. A global spectral model with a vertical finite element formulation for the vertical discretization: Adiabatic formulation. *Mon. Weather Rev.* **113**: 1910–1919.

BLECK, R. 1977. Numerical simulation of lee cyclogenesis in the Gulf of Genoa. *Mon. Weather Rev.* **105**: 428–445.

BOER, G.J.; N.A. McFARLANE, R. LAPRISE, J.D. HENDERSON and J.-P. BLANCHET. 1984. The Canadian Climate Centre Spectral Atmospheric General Circulation Model. ATMOSPHERE-OCEAN, **22**: 397–429.

CHOUINARD, C. 1984. A study of the systematic errors of the Canadian Meteorological Centre's Spectral Model. ATMOSPHERE-OCEAN, **22**: 226–243.

LILLY, D.K. 1972. Wave momentum flux — A GARP problem. *Bull. Am. Meteorol. Soc.* **53**: 17–23.

———, 1978. A severe downslope wind storm and aircraft turbulence event induced by a mountain wave. *J. Atmos. Sci.* **35**: 59–77.

———; J.M. NICHOLLS, R.M. CHERVIN, P.J. KENNEDY. and J.B. KLEMP. 1982. Aircraft measurements of wave momentum flux over the Colorado Rocky Mountains. *Q.J.R. Meteorol. Soc.* **108**: 625–642.

LINDZEN, R.S. 1981. Turbulence and stress owing to gravity wave and tidal breakdown. *J. Geophys. Res.* **86**: 9707–9714.

MESINGER, F. 1977. Forward-backward scheme, and its use in a limited-area model. *Beitr. Phys. Atmos.* **50**: 200–210.

PELTIER, W.R. and T.L. CLARK. 1979. The evolution and stability of finite-amplitude mountain waves. Part II: Surface wave drag and severe downslope windstorms, *J. Atmos. Sci.* **36**: 1498–1529.

——— and ———. 1983. Nonlinear mountain waves in two and three spatial dimensions. *Q.J.R. Meteorol. Soc.* **109**: 527–548.

PIERREHUMBERT, R.T. and B. WYMAN. 1985. Upstream effects of mesoscale mountains. *J. Atmos. Sci.* **42**: 977–1003.

SADOURNY, R. 1984. Midlatitude systematic errors in numerical models. *In*: GARP Spec. Rep. No. 43: Report of the Seminar on Progress in Numerical Modelling and the Understanding of Predictability as a Result of the Global Weather Experiment, October 1984, Sigtuna, Sweden, WMO/TD – No. 33, III, pp. 156–174.

WALLACE, J.; S. TIBALDI and A.J. SIMMONS. 1983. Reduction of the systematic forecast errors in the ECMWF model through the introduction of an envelope orography. *Q.J.R. Meteorol. Soc.* **109**: 683–717.